PATHOS FET-OPEN

European Commission

PHOTONIC AND NANOMETRIC HIGH-SENSITIVITY BIO-SENSING

DELIVERABLE 2.3 [HUJI, M46]
REPORT ON CHARACTERIZATION OF CORRELATED SPIN-BATH SPECTRA USING NV-CENTERS AND NMR FACILITIES

WEIZMANN INSTITUTE OF SCIENCE
INRiM ISTITUTO NAZIONALE DI RICERCA METROLOGICA
technische universität dortmund
THE HEBREW UNIVERSITY OF JERUSALEM

CHARACTERIZATION OF CORRELATED SPIN-BATH SPECTRA USING NV-CENTERS AND NMR FACILITIES

Work Package 2

Nir Bar-Gill, Hebrew University, Jerusalem, Israel
Lucio Frydman, Weizmann Institute of Science, Rehovot, Israel
John Howell, Hebrew University, Jerusalem, Israel

Project number: 828946
Project partners: UNIFI, Weizmann, INRiM, HUJI, TUDO

Contents

1 Executive Summary

As deliverable D2.3 we report on our results of using nitrogen vacancy (NV) centers, photonic systems and NMR study and characterize correlated spin-bath spectra:

- We present novel results on the characterization of spin bath dynamics using NV Ramsey measurements as a function of magnetic field, indicating correlated behavior and back-action.
- We describe NMR measurements whereby the "bath" (e.g., 1Hs in a polycrystalline powder) is used as magnification reporter for the evolution of dilute, low-sensitivity X (e.g., 13C) spins.
- We consider the fundamental roles of frequency versus phase in parameter estimation, specifically in the Sagnac effect. We describe a novel, ultra-sensitive gyroscope based on the extremely steep frequency-dependent gain of a liquid crystal light valve.

2 NV spin-bath dynamics

The NV center is coupled to the naturally occurring nuclear spin bath of surrounding 13C isotopes, appearing with a standard abundance of 1.1%. This nuclear spin bath of spin ½ nuclei is usually the main source of dephasing for the NV electronic spin, limiting its T_2^* coherence time.
We have characterized the effects and dynamics of this spin bath as a function of an applied static magnetic field, which tunes the resonance of the NV electronic spin (it also affects the nuclear spins but to a lesser extent due to their small gyromagnetic ratio).
Below we detail our system and measurement schemes, as well as the results and their analysis.
We stress that this work was initiated as part of PATHOS, starting from the first reporting period and still on-going. The first few data sets were obtained in the previous reporting period, while most of the data presented below is from the past several months.

2.1 Experimental system and characterization schemes

The measurements were performed using a home-built scanning confocal microscope with capabilities of delivering microwave (MW) pulses to a diamond sample (Figure 1). Excitation is accomplished using laser delivery at 532nm, and detection performed by a single photon counting module. An external static magnetic field was applied using a permanent neodymium magnet with positioning control stages to achieve magnetic field alignment with the NV center axis.

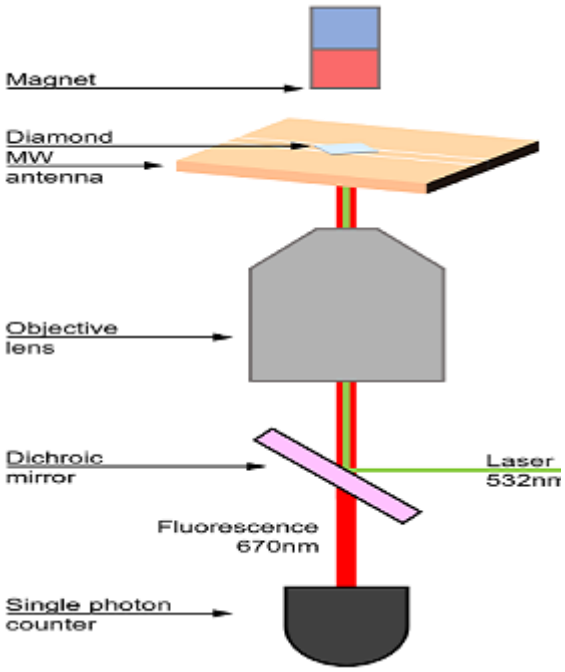

Figure 1: Schematic of the experimental system. Home-built confocal microscope with microwave delivery capabilities.

The experiment involves aligning a magnetic field and performing Ramsey sequences for varying values of free induction decay (FID) times. The Ramsey sequence is depicted in Figure 2, essentially consisting of the initialization of the NV spin to the symmetric superposition state, followed by a free

precession time τ, and finally a rotation back to the eigenstate basis and a measurement. This scheme provides a direct measure of the inhomogeneous dephasing time T_2^*.

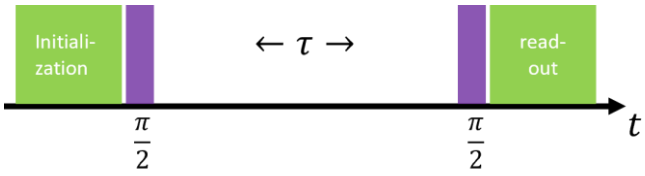

Figure 2: Ramsey sequence. The green pulses indicate laser pulses, while the purple indicate MW rotations. The FID precession time is varied and denoted as τ.

The MW pulses were applied with a controlled detuning from the NV resonance at each value of the magnetic field, in order to improve analysis accuracy. The results of each Ramsey sequence experiment (Figure 3) were fitted to the following model:

$$g(t) = e^{-\left(\frac{t}{T_2^*}\right)^n} (A_1 \cos(2\pi f t + \phi_1) + A_2 \cos(2\pi(f+3) + \phi_2)) + d$$

The model takes into account an NV center with an 15N nitrogen isotope; thus the two oscillating terms have a relative resonance shift of 3MHz due to the hyperfine interaction term. The decay is assumed to behave as a stretched exponential with the power n, which is related to the Markovianity (correlations) of the bath.

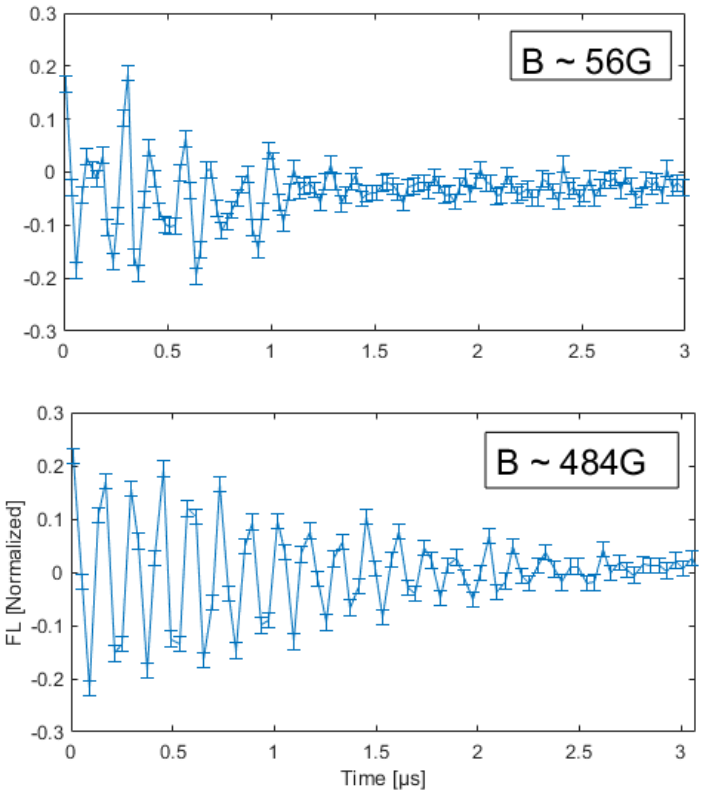

Figure 3: Representative Ramsey measurement results at two different values of the applied magnetic field. It can be seen that the coherent oscillations in the FID sustain for a longer coherence time at the field $B \sim 484G$, close to the excited-state level anti-crossing (ESLAC) of the NV (see text).

2.2 Results and analysis

Using the experimental system and techniques described above, we studied the dependence of the NV coherence time T_2^* on the externally applied magnetic field (Figure 4). We compared results measured on several NVs, including NVs occurring in a standard diamond substrate with a natural abundance of 13C nuclear spins (denoted as "Lucky") vs. NVs in an isotopically purified diamond sample, in which the 13C concentration is negligible (denoted as "Or").

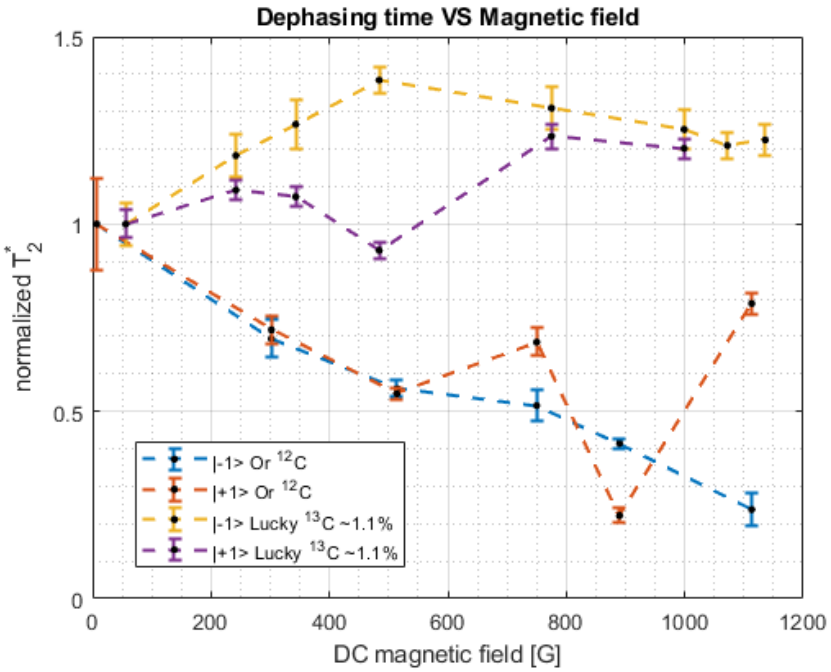

Figure 4: Measured normalized T_2^* coherence times (to the value at low field) as a function of the externally applied static magnetic field, for both the $+1$ and -1 states of the NVs, and for NVs in a diamond sample with a natural abundance of 13C ("Lucky") vs. an isotopically purified sample with a negligible 13C concentration ("Or").

We find that the coherence time in the normal sample increases for larger field, and specifically for field values near the excited-state level anti-crossing (ESLAC) around 500 G for the -1 state.

We therefore hypothesize that near the ESLAC the NV induces polarization in the 13C bath, and due to the backaction of the bath on the NV we observe an enhanced coherence time. This is supported by the fact that such an effect should be more pronounced for a denser 13C nuclear spin bath, as can be seen in the comparison between the two samples (Figure 4).

Such polarization can be induced due to a resonance condition between the NV electronic spin and the 13C nuclear spins, which occurs at the ESLAC (). Due to the Zeeman effect, applying an external magnetic field B_0 tunes the NV electronic spin resonance according to:

$$E_{NV} = D_{es} - \gamma_e B_0$$

Where D_{es} is the excited state resonance at zero magnetic field, and γ_e is the electronic gyromagnetic ratio for the NV spin.
The Hamiltonian describing the system of an NV in the electronic excited manifold and a nearby 13C nuclear spin is

$$H = D_{es}S_z^2 + \gamma_e B_0 S_z + \gamma_n B_0 I_Z + A_\parallel (S_z I_z) + A_\perp (S_+ I_- + H.C.)$$

Where γ_n is the nuclear gyromagnetic ratio, $A_\parallel, A_\perp$ are the parallel and perpendicular hyperfine coupling strengths, S are the NV electronic spin operators and I are the 13C nuclear spin operators.

3 Spin-bath correlations in NMR systems – the bath as a reporter

Chemical exchange saturation transfer (CEST) is a widely used technique for enhancing the sensitivity of liquid-state NMR spectra; its main applications involve the magnified detection of metabolites and bio-macromolecules *in vivo*, the detection of "invisible" states in high-resolution biomolecular NMR, studies of exchange and enzymatic phenomena *in vitro*, and NMR enhancements of hyperpolarized substrates. CEST involves selectively saturating weak NMR resonances of labile or otherwise interconverting sites, and then relying on chemical exchange processes to transfer this site-selective saturation onto a much stronger NMR resonance. By leveraging the fact that the rate k_{exch} of this exchange process can be much faster than the longitudinal relaxation rate $1/T_1$ of the receiving pool, which is ultimately excited and detected, this saturation-transfer principle can lead to very large sensitivity enhancements on the order of $k_{exch} \cdot T_1$. It follows that, when discussing CEST experiments, it is useful to classify the chemical exchanging spin system into two distinct pools based on their relative populations and on their overall NMR receptivity. Spins giving NMR signals that are of interest, but are weak as a result from low natural abundance, small gyromagnetic ratios, low concentrations, and/or combinations of all these, constitute what we will call the *magnetically dilute* spin pool. This will in turn exchange information with the *magnetically abundant* spin pool, a highly populated and easier to detect reservoir (like the protons in water). Given the ease and robustness with which CEST can be implemented, as well as the large gains in sensitivity that it can provide, CEST has since been exploited in the above-mentioned variety of liquid-state and *in vivo* NMR scenarios – providing a wealth of information pertaining to structure and dynamics.

As originally introduced, CEST is a continuous-wave (CW), frequency-domain experiment targeting what is usually a peak of interest whose resonance frequency is *a priori* known. *Frequency Labeled EXchange* (FLEX) endows CEST with the broadbandness associated with time-domain experiments. In FLEX, the resonances of the dilute pool are not saturated, but rather amplitude-modulated by a pair of selective excitation/storage pulses that avoid perturbing the abundant spin reservoir. These pulses are separated by a t_1 delay that is incremented in a normal 2D NMR fashion but which, unlike conventional 2D NMR, is looped multiple times before the final observation. This allows the chemical exchange process to transfer the t_1 information onto the abundant reservoir as a magnified amplitude modulation that grows with the number of loops; applying an observation pulse on the abundant reservoir then enables, after Fourier Transform (FT) *vs*. t_1, the detection of the dilute pool NMR spectrum with an increased, CEST-like sensitivity. By departing from the original CW saturation scheme, FLEX provides this experiment with additional flexibility. Recently, for example, sensitivity-enhanced solution-state NMR pulse sequences have been developed that exploit this approach for increasing the SNR of not only labile protons, but also the SNR of non-labile (*e.g.*, aliphatic) protons as well as non-labile heteronuclei (^{13}C, ^{15}N) for a variety of systems including carbohydrates, amino acids, and intrinsically disordered proteins. Some of these experiments also depart from traditional CW CEST approaches in that following the t_1 time-domain encoding, they rely not only on chemical exchange but also on coherent (*e.g.*, TOCSY, INEPT) polarization transfer segments to achieve their substantial signal enhancements in either homonuclear or heteronuclear systems, starting from either labile or non-labile spins. Inspired by these solution-state RElayed-FLEX (REFLEX) sequences, we herein explore and test a protocol for implementing conceptually similar experiments, but aimed at acquiring NMR spectra from solid samples undergoing magic-angle-spinning (MAS) and heteronuclear decoupling. As in the solution-state REFLEX counterparts, the aim of these methods will be to enhance 2D heteronuclear spin correlation (HETCOR) experiments involving dilute nuclei like ^{13}C; unlike the solution-state NMR cases, no chemical exchanges with a dominating solvent will be available for use, and acquisitions will have to be done under the stringent decoupling and spinning manipulations that are needed for collecting high-resolution NMR spectra from powdered solids.

The results presented here are further detailed in the published reference [1].

3.1 Fourier-Encoded Saturation Transfer in High-Resolution Solid-State NMR

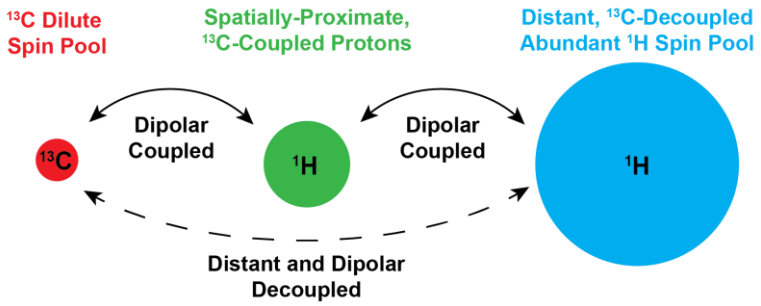

Figure 5: Schematic representation of how a typical organic solid can be formalized in terms of three distinct spin pools (indicated by the different colors), each with varying populations and receptivities (indicated by the size of the circles). The system entails a 13C (red) that is dipole-coupled to a proximate proton (green), with the latter dipolar-coupled with an abundant 1H spin bath (in blue) that is not directly coupled to the heteronucleus, but whose observation is key for enhancing the NMR signal of the 13C spin.

A Fourier-encoded, solid-state NMR version of FLEX. To extend the solution-phase saturation transfer principles described above to solids undergoing both heteronuclear ^{1}H decoupling and MAS, we put forward the *Fourier-Encoded Saturation Transfer* (FEST) experiment. FEST is in principle applicable to the observation of any *X*-nucleus surrounded by a ^{1}H reservoir; here we target dilute ^{13}C surrounded by an ensemble of abundant protons as a representative example. The are several conceptual elements of FEST experiments that have both similarities and differences to the elements involved in solution-state CEST/FLEX NMR; hence they are introduced in this paragraph one by one. The enabling component of FEST are dipolar couplings –both those between the dilute ^{13}Cs and its neighboring, strongly coupled ^{1}Hs, as well as those between these ^{13}C-coupled ^{1}Hs and the ^{1}H bulk ensemble at large. ^{13}C-^{1}H dipolar couplings are normally used in conventional 2D HETCOR solids NMR for sensitizing experiments, for instance upon pre-polarizing the ^{13}C *via* cross-polarization (CP), and/or when transferring back the ^{13}C encoding to perform ^{1}H-detection with enhanced sensitivity. However, by virtue of their separation and of the low ^{13}C natural abundance, these dipolar-driven processes will involve only a small fraction of the total protons in the sample, as most ^{1}Hs are not coupled strongly enough to the carbon in order to participate in polarization transfers. Therefore, this abundant ^{1}H spin polarization goes largely unused. FEST seeks to exploit this large portion of the abundant ^{1}H spin system as part of the signal enhancement process, by making *it* the reporter of the ^{13}C NMR time-domain FID. To do so the proposed experiment relies on the REFLEX-inspired approach introduced in **Figure 5**. This depicts a typical organic solid in terms of three spin pools, each having varying populations and receptivities schematically illustrated by the size of their circles: the ^{13}C, the ^{1}H(s) that is(are) strongly coupled to the ^{13}C, and a more abundant, essentially ^{13}C-decoupled ^{1}H reservoir, that will make the bulk of the NMR signal in a ^{1}H-detected experiment. Further, it is assumed that the distinct dipolar couplings that exist between these various spin pools allows each to be individually addressed with suitable radio-frequency (RF) manipulations; for instance, CP can be used to transfer polarization between ^{13}C and its directly dipole-coupled ^{1}Hs, while spontaneous or RF-driven spin diffusion enables the communication between the latter ^{1}Hs and the much larger portion of the abundant ^{1}H spin pool (shown in blue).

With this as background, the procedure by which we propose to use the latter for efficiently enhancing the dilute ^{13}C NMR signature is described in **Figure 6(a-d)**. According to this scheme, (1) the proximate ^{1}H pool is first used to polarize the ^{13}C; (2) the latter's time-domain evolution is triggered, encoded over a time t_1, and then passed back onto ^{1}H$^{(proximate)}$ as an amplitude modulation; (3) a ^{1}H-^{1}H spin-diffusion interval is allowed to proceed whereby this proximate ^{1}H pool depolarizes the distant ^{1}H$^{(abundant)}$ to a degree that reflects the ^{13}C t_1 evolution while getting repolarized in exchange; (4) the whole process is repeated several times, so as to imprint the ^{13}C evolution onto the bulk ^{1}H reservoir to the maximum possible extent. Step (2) acts here as the Fourier-encoding module in FLEX, while steps (3) and (4) would act as analogues of the chemical exchange saturation transfer process amplifying the signal. The ^{13}C signal magnification that these processes bring about

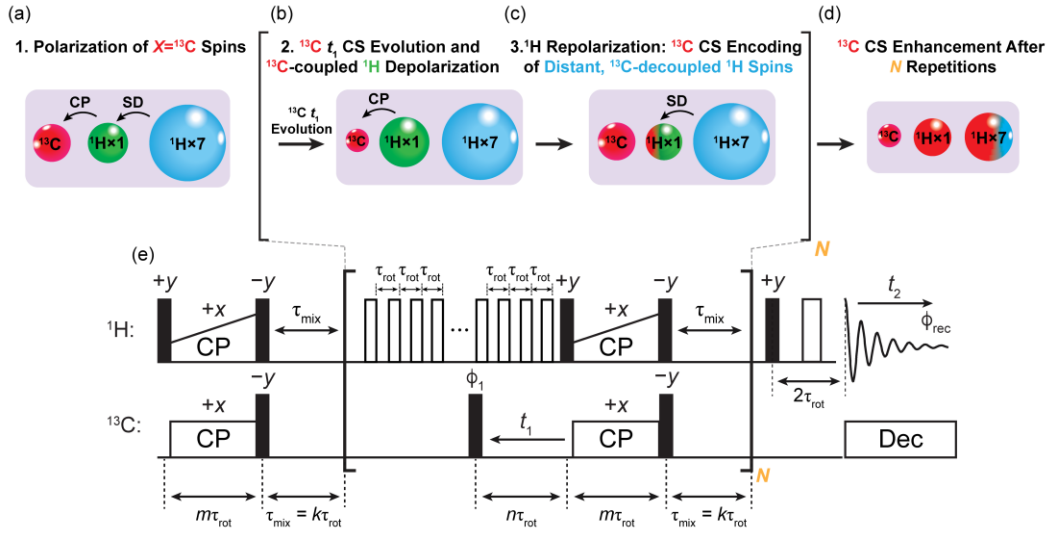

Figure 6: Schematic representation of the (a-d) spin dynamics over the course of the (e) Fourier-Encoded Saturation Transfer (FEST) pulse sequence. The magnetically dilute 13C spin pool, spatially-proximate 13C-coupled 1H spin pool, and the magnetically-abundant 13C-decoupled 1H spin pool, are represented in red, green, and blue, respectively. Colors are also used to represent the distinct spin pools and the size of the nuclei indicate the relative magnetizations. Cross polarization (CP) transfer and 1H-1H spin diffusion (SD) processes are indicated with black arrows; see text for a more detailed explanation. Black and white pulses in (e) denote calibrated π/2 and π pulses, respectively whose phases are indicated when relevant. The CP contacts along with the mixing interval, t1 evolution time, and associated decoupling period are all rotor synchronized: m, k, and n are integers and τrot is the rotor period. A rotor synchronized Hahn echo is also used to excite the final 1H observable.

will depend on the number of times that the overall process is repeated, on the degree of ^{13}C *vs*. ^{1}H (bulk) dilution, on the strength of the couplings between the various pools, on the longitudinal ^{1}H and ^{13}C T_1 and $T_{1\rho}$ relaxation-time constants, and on the efficiency with which all these processes can be implemented while under the high-resolution requirements of solid-state ^{13}C NMR.

Figure 6e introduces a time-domain pulse sequence that could be used for magnifying in this manner the chemical shift modulation of a dilute ^{13}C spin pool on a more abundant bulk ^{1}H reservoir –while remaining compatible with the decoupling and MAS demands imposed by high resolution ^{13}C observations. The steps that are involved in the ensuing indirect-detection sequence, as well as their approximate correlation with the processes introduced in **Figure 6(a-d)**, include: (1) An initial block where polarization is received by the ^{13}C from its proximate, dipolar-coupled ^{1}H *via* an optimized CP process, which is long enough to be effective, but also short so as to not incur detrimental $T_{1\rho}$ ^{1}H relaxation losses. Particularly important is the preservation of the spin polarization belonging to the abundant proton pool, which is therefore stored post-CP along the +*z* axis. (2) This is followed by a mixing interval τ_{mix} that is sufficiently long for enabling ^{1}H-^{1}H spin-diffusion yet short *vs* the ^{13}C T_1, so that the ^{13}C remain fully polarized at the end of τ_{mix}, while spin polarization from $^{1}H^{(abundant)}$ spontaneously repolarizes the depleted ^{13}C-coupled proton through spin diffusion. (3) In a process that will be repeatedly executed, the ^{13}C longitudinal spin polarization is excited and allowed to evolve for a short t_1 increment (≈µs-ms, best performed in a constant-time 2D fashion for t_1-noise reduction) under the effects of a heteronuclear decoupling sequence that removes the effects of $^{1}H^{(proximate)}$ –while taking care to not significantly affect the bulk proton magnetization. At the end of the t_1 evolution time, the ^{13}C magnetization is once again put into Hartmann-Hahn contact with its neighbouring proton, which had in the preceding τ_{mix} and t_1 periods been repolarized. During this CP process the ^{13}C-coupled $^{1}H^{(proximate)}$ will be depolarized, by an amount that depends on the modulation imposed by the t_1 ^{13}C chemical shift evolution. Once again, care is here taken to ensure that the protons of the abundant spin pool, which are not dipolar-coupled to ^{13}C, remain as unaffected by this CP contact as possible. (4) Following this point, the spin polarization of the ^{13}C-coupled $^{1}H^{(proximate)}$, which has now been depleted by an amount that depends on the ^{13}C's t_1 evolution, is repolarized *via* spin-diffusion over a new mixing time τ_{mix} in a manner analogous to that described above in step 2. However, a key difference in this case is that it will now be *the longitudinal spin polarization of the $^{1}H^{(abundant)}$ spin pool, that will be depleted by an amount depending on the ^{13}C's chemical shift t_1 evolution*. Repeating steps 3-4 numerous (*N*) times per scan up to a point

dictated by the T_1 and $T_{1\rho}$ relaxation constraints of the ^{1}H and ^{13}C spin systems should thus lead to an appreciable depletion of the ^{1}H polarization, in a ^{13}C chemical-shift-dependent fashion. A final excitation pulse measuring the ensuing abundant ^{1}H reservoir polarization then reveals the ^{13}C t_1 modulation, which when incremented translates an entire ^{13}C NMR time-domain (FID) signal as a modulation of the full proton reservoir response.

FEST NMR: Numerical Simulations. This approach to amplify and detect ^{13}C chemical shifts in a natural abundance solid was numerically tested with idealized quantum-based density matrix simulations, carried out using custom-written code. These simulations were performed for a polycrystalline powder assumed to be undergoing MAS at ν_{rot} = 40 kHz, and for simplicity we assumed that the three spin pools schematically indicated by the three different colours in **Figure 6(a-d)** possessed a distinct, uniquely addressable chemical shift: the abundant and dilute proton pools were set to $\nu(^1H)^{(abundant)}$ = 0 kHz and $\nu(^1H)^{(proximate)}$ = 10 kHz. These pools were composed of 7 and 1 ^{1}H spins, respectively; a single ^{13}C was dipole-coupled solely to the latter ^{1}H and given an offset $\nu(^{13}C)$ = 2 kHz. The spin dynamics imposed by the FEST pulse sequence (**Figure 6e**) were then simulated on this spin ensemble and, *in lieu* of the final ^{1}H excitation pulse, the expectation value of the abundant spin pool's *z*-polarization $\langle \hat{I}_z^{(abundant)} \rangle$ was monitored as a function of the number of FEST loops (N) and of the ^{13}C t_1 evolution time. **Figure 7a** shows these expectation values, as calculated at the end of the last mixing interval in the sequence. The black curve in this figure shows the t_1-dependent trajectory of the *x* ^{13}C spin polarization component, $\langle \hat{S}_x^C(t_1) \rangle$, that results immediately after a single CP contact. This would be the conventionally detected signal in an indirectly-detected heteronuclear correlation experiment, and its clear 2 kHz frequency modulation serves as our reference. Calculated $\langle \hat{I}_z^{(\mathrm{abundant})}(t_1) \rangle$ expectation values normalized with respect to this $\langle \hat{S}_x^C(t_1) \rangle$'s modulation as a function of looping are shown in other colours in this panel. Note that losses derived from pulse non-idealities and/or relaxation processes are here ignored, as are enhancements resulting from differences in the gyromagnetic ratios (*i.e.*, $\gamma(^1H)/\gamma(^{13}C)$). In other words, any modulation larger than ±0.5 represents a net signal enhancement over an indirect ^{1}H-detected experiment. **Figure 7a** confirms that the ^{13}C chemical shift modulation is ported with magnification onto the ^{13}C-decoupled, abundant ^{1}H spin pool; this corroborates **Figure 5's** model, whereby a ^{1}H→^{13}C→^{1}H CP transfer and subsequent ^{1}H-^{1}H spin diffusion processes allow one to impart the ^{13}C-modulation even on distant, dipolar-decoupled spin pools under fast MAS rotation. Notice that this ^{13}C-derived, $^1H^{(abundant)}$-detected modulation increases in amplitude as the number of loops N increases, as does the concomitant depletion of the abundant spin pool's polarization. At

some point, however, the FEST looping leads to deviations from the ideal sinusoidal t_1-modulation; this $\langle \hat{I}_z^{(\mathrm{abundant})}(t_1) \rangle$ distortion for large values of *N* reflects the small spin system here assumed and the lack of relaxation processes, which imposes non-linearities between the extent of the ^{13}C-imposed modulation and the signal enhancement afforded by the ^{1}Hs. While we have observed this behavior in certain solution-state, J-based analogues of this experiment (data not shown), we have not seen such distortions in the solid-state NMR measurements described below, presumably due to the extended nature of the spin-coupled solids network and the effects of spin relaxation. **Figure 7b** examines the maximum enhancement of the ^{13}C-modulation, showing that in the absence of relaxation it will ultimately depend on the number of spins in the abundant ^{1}H pool. In general, the maximum modulation depth will be given by half the number of ^{1}H spins in this pool; given the ^{13}C dilution at its natural abundance, this means that the potential ^{13}C signal magnification afforded by FEST in organic solids can be very large. The actual conditions at which the maximum ^{13}C enhancement will be achieved and its signal magnification value will depend on additional factors, including the ^{1}H/^{13}C T_1 relaxation times and the effective internuclear dipolar couplings.

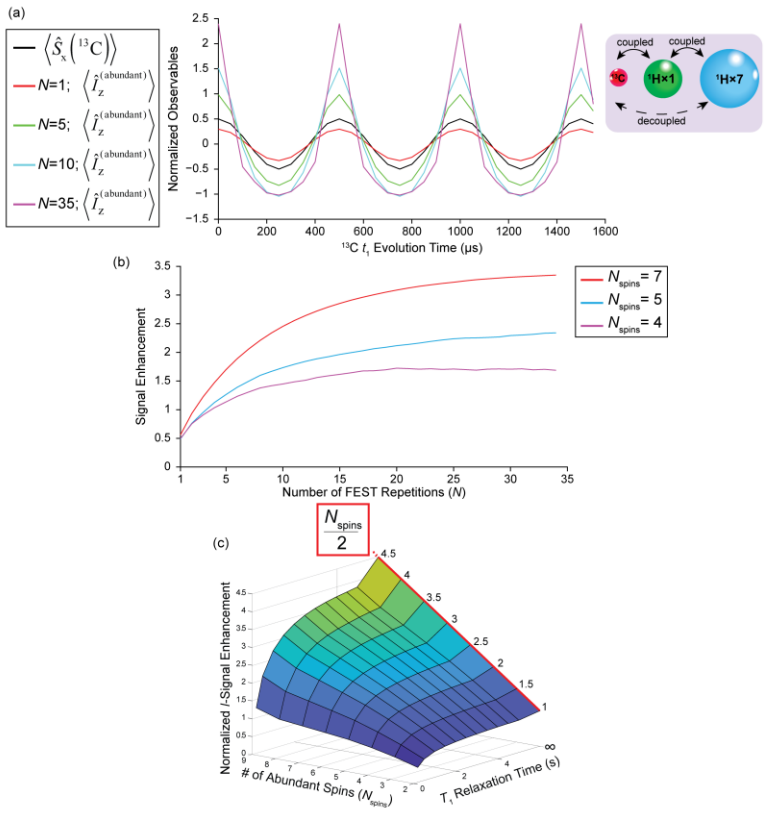

Figure 7: (a) Quantum mechanical (SIMPSON) simulations showing the time-dependent expectation values of ⟨Ŝ_x^((13C))⟩ (black trace) for 13C after a single CP contact and ⟨Î_z^((abundant))⟩ for the seven protons comprising the abundant spin pool introduced in Figure 1. ⟨Î_z^((abundant))⟩ is calculated at the end of the mixing int¬¬erval for different values of FEST repetitions (N). The isotropic shifts of the abundant and dilute spin pools were set to 0 kHz and 2 kHz, respectively and a t1 increment of Δt1 = 50 μs was used with a total of 32 t1 points simulated. Homonuclear dipolar coupling constants of 2.5, 12, and 22 kHz were employed along with a single heteronuclear 1H-13C dipolar coupling constant of 15 kHz. 100 kHz RF fields were used in all cases for all excitation and storage pulses and spin locking RF fields v1(1H) = 100 kHz and v1(13C) = 60 kHz were assumed for CP. Rotor synchronized radio-frequency driven recoupling (RFDR)40 was used to achieve efficient homonuclear mixing in τmix = 4 ms. Ideal decoupling was assumed during the t1 evolution period by explicitly supressing the heteronuclear dipolar coupling Hamiltonian. A spinning speed of vrot = 40 kHz was assumed and the average over the powder was calculated using 10 (α,β) crystallites sampled according to the REPULSION scheme.41 (b) Signal enhancement of the 13C shift modulation detected in Î_z^((abundant)) as a function of N and of the number of spins composing the abundant spin pool (i.e., Nspins), arising from identical simulation parameters as in (a). (c) Normalized signal enhancements predicted for a two-site system incorporating a single modulated I(proximate) spin in chemical exchange with a larger I(abundant) reservoir containing Nspins, assuming four distinct exchange rates varying between 2-10 kHz. Bloch-McConnell equations were used to extract this as a function of Nspins as well as of T1(1H) relaxation time.

3.2 Experimental Section

Samples of ibuprofen and sucrose were purchased from Sigma-Aldrich; L-Histidine HCl was purchased from B.D.H Laboratories. All were used as received without further purification. Samples were ground into fine powders and packed in 1.6 mm zirconium NMR rotors for measurement. NMR experiments were performed using a Varian VNMRS console interfaced to an Oxford 14.1 T (ν0(1H) = 600 MHz) wide-bore magnet. A Varian 1.6 mm triple-resonance HXY MAS probe was used for all NMR experiments. All spectra were acquired at a spinning speed of νrot = 40 kHz with a stability of ±5 Hz, using active pulse triggering and temperature regulation at 20° C. The magic angle of the probe was calibrated to 54.74° by maximizing the number of rotational echoes observed in the 81Br FID of KBr. 1H and 13C pulse width calibrations were performed using a sample of adamantane (40 kHz MAS), which was also used for chemical shift referencing. 1H→13C{1H} transfers were first calibrated using conventional CPMAS pulse sequences on each individual sample; contact times and spin-locking radiofrequency (RF) field strengths were then further refined in each 2D NMR experiment for the first t1=0 increment. Rotary-resonance recoupling conditions employed in 2D indirectly-detected heteronuclear correlation (idHETCOR) experiments to suppress unwanted background signals were experimentally optimized by adjusting the length and power of the orthogonal recoupling pulses and then measuring the resulting 1H NMR spectra. All 2D NMR experiments used the same heteronuclear π-based decoupling sequence, which gave optimized decoupling conditions, and had their t1 evolution periods synchronized with the spinning frequency. Optimizing the FEST experiments required determining the mixing time (i.e., τmix) and number of loops (i.e., N) combination that resulted in the largest overall depletion of the 1H spin polarization. This was done by repeatedly depolarizing proton magnetization via multiple-contact 1H-13C CP for a fixed N/τmix combination, and then measuring the resulting 1H signal; this gave a so-called S(on) dataset. Repeating this under identical experimental conditions but in the absence of 13C spin-locking pulses gave a so-called S(off) dataset. Plotting {S(off)-S(on)}/S(off) as a function of both N and

τmix revealed the percentage of protons that was depleted; the largest value of this parameter gives the largest overall enhancement in terms of 13C SNR.

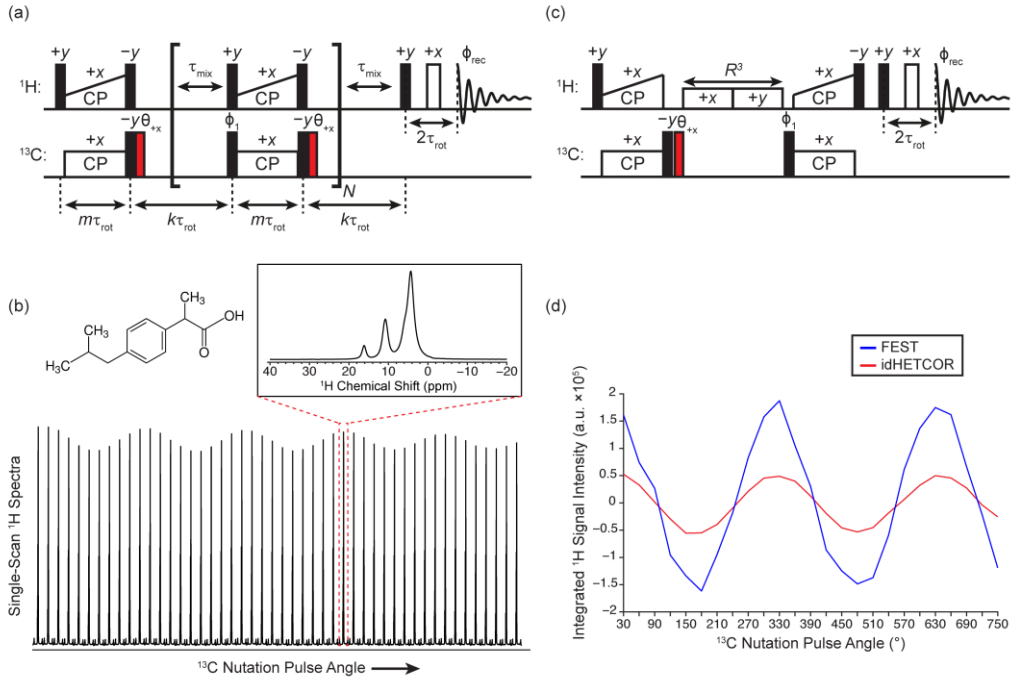

Figure 8: (a) Schematic representation of a modified FEST pulse sequence whereby a 13C nutation pulse (shown in red) encodes the 13C nutation frequency onto both 13C-coupled and 13C-decoupled protons. (b) Experimental 1H single-scan nutation-encoded FEST spectra collected using a naturally-abundant ibuprofen sample (vrot = 40 kHz, Bo=14.1 T) as a function of the 13C nutation angle, which is increasing in 30° steps from 0 to 1410°, for N = 20 loops and τmix = 10 ms. The inset shows a representative 1H NMR spectrum at a particular 13C nutation angle. (c) Schematic representation of an optimized comparison consisting of a modified, nutation-encoded idHETCOR pulse sequence. This modified idHETCOR pulse sequence begins by exciting proton-coupled 13C spins with 1H-13C CP and then encoding these same strongly-coupled protons with the 13C nutation frequency using 13C-1H back CP. A rotary-resonance recoupling period placed between the CP contacts reintroduces proton homonuclear dipolar couplings that serve to rapidly de-phase any remaining transverse proton spin polarization, which ensures 13C polarization flows to proximate protons during back CP.35 An added advantage of this dipolar recoupling period is an immunity against t1 noise (vide infra). (d) Integrated 1H signal intensities collected with phase cycling (4 scans in both cases) using FEST (blue) and idHETCOR (red) on the same ibuprofen sample as (b).

3.3 Results

FEST NMR Experiments. Having devised a way whereby ^{13}C offsets can be imparted onto a distant abundant spin pool while under the effects of heteronuclear decoupling and MAS by exploiting the repeated depolarization/repolarization of a directly-bonded, mutually-coupled proton, a series of experimental tests were performed to corroborate these numerical predictions. These experiments were performed on the basis of auxiliary optimizations of the CP and mixing conditions\. Shown as an initial experimental test is a simpler version of the FEST sequence (**Figure 8a**), where the ^{13}C t_1 evolution is replaced by a variable-angle ^{13}C nutation pulse θ (in red). This pulse modulates all ^{13}C spins to the same extent (*i.e.*, at a single frequency), which can then be easily seen in the bulk, single-scan ^{1}H NMR signal as the ^{13}C nutation pulse is incremented in a pseudo 2D fashion (**Figure 8b**). As expected the spin dynamics are such that when the ^{13}C nutation angle is 0 or an integer multiple of 2π, the ^{13}C polarization that is spin locked in the looped CP processes is maximal; consequently, these angles result in the *least* amount of bulk ^{1}H depolarization. By contrast, when θ(^{13}C) is an integer multiple of π, the ^{13}C spin polarization is stored along the −*z* axis after the first CP and is therefore, antiparallel with respect to its spin locking B_1 field during subsequent Hartmann-Hahn contacts; this

results in the *largest* depolarization of the ^{1}H bulk signal. Notice that all other values of θ(^{13}C) depolarize the bulk ^{1}H spins in the expected cos(θ)-dependent manner, with no evidence of the small-reservoir distortions noted in **Figure 7**; this is a consequence of the small ^{13}C/^{1}H ratio in this polycrystalline natural-abundance sample. Notice as well the strength of the FEST effect, which is sufficient to easily detect the ^{13}C nutation frequency in these single-scan bulk proton signals, and is akin to what we have observed in water-based ^{1}H CEST observations of non-labile ^{13}C NMR spectra. It is possible to approximately estimate the degree of the enhancement in the FEST MAS experiments, by comparing their modulation against that which can be indirectly detected in ^{13}C-filtered polarization, by appropriate phase cycling of the ^{13}C excitation pulse that precedes CP. The result of this is a modified idHETCOR pulse sequence, whereby the t_1 evolution period has been replaced with a ^{13}C nutation pulse (**Figure 8c**). **Figure 8d** shows *ca*. a 3× signal enhancement achieved with FEST over an idHETCOR, with both datasets acquired under similarly optimized experimental conditions.

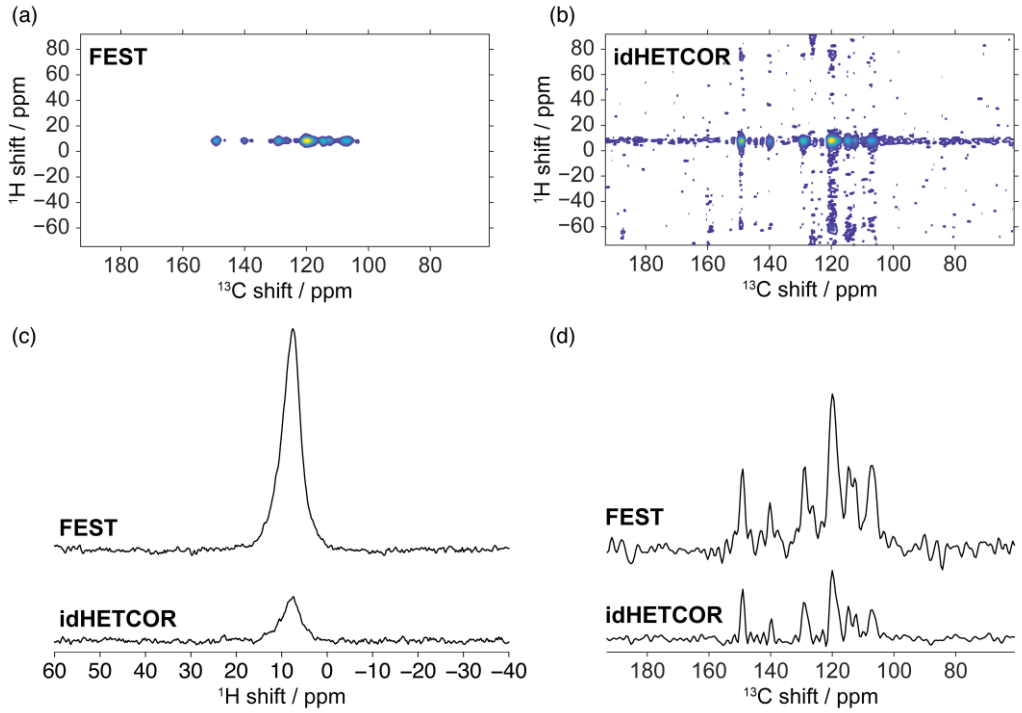

Figure 9: Experimental proton-detected 1H-13C correlation spectra of naturally abundant sucrose (vrot = 40 kHz) collected with (a) FEST (τmix = ca. 100 ms, N=15) and (b) idHETCOR in 2 scans and 4 scans, respectively (recycle time is 60 s for both and a total of 64 t1 points were collected under optimized experimental conditions). (c) 1H NMR spectra collected for the first t1 increment using (top) FEST and (bottom) idHETCOR. (d) 13C F1 slices taken from the same F2 point in the 2D spectra for (top) FEST and (bottom) idHETCOR. The minimum, maximum, and spacing of contour levels is set based on the standard deviation of the noise in each dataset.

Experimental tests were also performed to explore FEST's ability to read-out site-resolved ^{13}C NMR spectra in this manner. **Figure 9** compares FEST NMR results obtained on a polycrystalline sample of naturally-abundant sucrose, *vs.* results from an optimized version of the idHETCOR sequence. The resulting 2D FEST spectrum (**Figure 9a**) consists of the single broad peak characteristic of the bulk ^{1}Hs observed under MAS conditions along the direct (F_2) dimension, showing strong correlations to seven ^{13}C resonances observed in the indirect (F_1) dimension. A signal amplification of *ca*. 7× is achieved against the optimized 2D idHETCOR counterpart (**Figure 9b**), which is also visible by comparing the ^{1}H NMR spectra acquired for the first t_1=0 increment of FEST and idHETCOR (**Figure 9c**, top and bottom, respectively). Notice that in all cases, the FEST experiment highlights both protonated and non-protonated ^{13}Cs owing to its reliance on relatively long CP times.

The primary challenge facing the sensitivity enhancement achievable from these ^{13}C-shift-encoded FEST experiments, turned out to be choosing an optimized heteronuclear dipolar decoupling sequence during the t_1 evolution period. Such a sequence has to deliver a high-resolution ^{13}C NMR

spectrum without ^{1}H coupling artifacts or broadenings, while at the same time preserving and leaving the abundant ^{1}H spin polarization "untouched", which will eventually be the source of any ^{13}C FEST enhancement. Any scan-to-scan instability in the performance of this heteronuclear t_1-decoupling sequence, led to unacceptable amplifications in the t_1 noise. Our final selection was a π-based, constant-time heteronuclear dipolar decoupling sequence, involving repeated units of 8 short, high-power, rotor-synchronized ^{1}H π-pulses applied at the end of a rotor period, with their phases XY8 phase-cycled. The overall number of ^{1}H decoupling pulses were thus kept constant, and the effective ^{13}C evolution time was defined by "walking" the ^{13}C excitation pulse throughout this period, in increments matching the XY8 decoupling subunits. This procedure led to penalties both in terms of sensitivity losses associated to the constant-time operation, partial saturation of the ^{1}H reservoir, and the introduction of scan-to-scan instabilities leading to t_1 noise –but it was the best we managed to devise.

3.4 Discussion and Conclusions

The present study put forward a time-domain, CEST-inspired experiment, for increasing the sensitivity of solid-state HETCOR NMR experiments. Unlike liquid-state CEST, which relies on actual chemical exchanges to facilitate the transfer of chemical shift information between a magnetically dilute spin pool and an abundant water spin pool, the FEST experiments here presented rely on an abundant ^{1}H reservoir for achieving its sensitivity enhancement, and on the discriminated use of heteronuclear and homonuclear dipolar couplings for driving the various transfers of polarization/saturation. The former is used, *via* CP contacts, to translate the heteronuclear chemical shift encoding into proton depolarization, while spin diffusion is used to extend this depletion throughout distant protons, for the sake of achieving sensitivity enhancement. In this fashion, FEST experiments performed on naturally-abundant organic compounds allow for the nutation or shift modulation of a magnetically dilute ^{13}C spin pool to be encoded onto a magnetically abundant ^{1}H spin pool. In parallel to what was exploited in the solution-state REFLEX experiment, a defining feature of FEST is the conceptual separation between magnetically dilute ^{1}Hs that are strongly dipolar-coupled with the heteronucleus, and the abundant, essentially ^{13}C-decoupled ^{1}H spin reservoir whose depletion will eventually lead to the signal enhancement. In the solution-state NMR case, the former were given by labile ^{1}Hs that are *J*-coupled to the heteronucleus, but also capable of exchanging with the water pool; in the latter their definition is less clear, as the "dilute" ^{1}Hs are defined by the pool of spins that can cross-polarize to/from a given ^{13}C site, while the "abundant" ^{1}Hs are those parts of the larger network that has so far remained mostly passive in heteronuclear NMR. In the case of naturally-abundant organic solids it is clear that the latter will entail a larger majority of protons, opening a new route to a more efficient use of these abundant species' polarization for enhancing heteronuclear NMR. The present study relied on spontaneous spin-diffusion for the relay of polarization between the dilute and abundant ^{1}H spin reservoirs; it is conceivable that, particularly at the faster MAS rates that should facilitate this experiment, RF-assisted approaches might enhance the effectiveness of this process (in fact the train of π-pulses inserted during the t_1 period for heteronuclear decoupling, facilitated this *via* an RFDR-like mechanism).

As mentioned, the main limitation of the sequence that we devised was its high sensitivity towards t_1 noise artifacts, which clearly lowered the apparent gains of the experiment. These arose from fluctuations in the scan-to-scan intensities of the bulk ^{1}H NMR signals, which we ascribe mostly to inconsistencies brought about by the hundreds of ^{1}H π-pulses applied to achieve heteronuclear decoupling during t_1. These instabilities greatly decreased upon rotor-synchronizing the whole sequence, which included the synchronization of all events to the same initial sample rotor phase and by actively regulating the sample temperature. Nevertheless, despite these efforts, multiplicative t_1 noise artifacts were still observed in the final bulk ^{1}H signal. This can be clearly appreciated in the ^{13}C F_1 trace taken from the 2D FEST spectrum (**Figure 9d**, top) that, unlike the idHETCOR counterpart (**Figure 9d**, bottom), features strong t_1 noise ridges. Furthermore, the application of common strategies like rotary-resonance recoupling or phase cycling procedures to destroy ^{1}H spin polarization that has not been modulated over t_1, cannot be used in FEST, as this

would eliminate any potential signal enhancement. Alternative methods to attenuate the F_1 artifacts are currently being developed and tested. These include saturation-transfer methods that progressively deplete the abundant proton reservoir while invoking dipolar-order-mediated CP –a strategy proven effective at reducing t_1-noises when targeting NMR spectra under static conditions. Such dipolar-order states have also been reported for rotating solids, opening an interesting alternative for FEST experiments. Using such protocols under conditions of fast (ν_{rot} > 60 kHz) MAS could also alleviate the need for heteronuclear decoupling during the t_1 evolution, thereby greatly reducing the t_1 noise distortions affecting the ^{1}H-decoupled CP FEST experiments here described. Alternative sequences performed at fast spinning rates but operating on the basis of *J*- instead of dipolar-transfers, could further reduce t_1 noise artifacts. Efforts are underway to implement these, as well as customized denoising approaches based on data post-processing routines. Despite these current limitations and needs for improvement, FEST seems to open hitherto untapped sensitivity enhancements in solid-state high-resolution NMR, by the efficient use of abundant spin polarization that typically goes unused. Extensions of similar ideas to solution-phase experiments involving natural-abundance (non-exchanging) organic substrates, are also being explored.

4 Doppler Gyroscopes: A Novel Application of Spectral Correlations

One of the key aspects of the PATHOS program is studying correlations, temporal and spectral to unlock information about a system. We believe we have solved a critical debate that has lasted almost a century by using spectral correlations – are frequency shifts fundamental to the Sagnac effect?

The burgeoning field of quantum metrology seeks to find "quantum advantages" over existing classical measurement schemes. Owing to its importance in gyroscopes and gravitational wave detection as well as its fundamental nature in all branches of interferometry, phase estimation beyond the standard quantum limit has been the prototypical example. Pragmatically, due to loss, quantum phase estimation techniques have, so far, only offered a few percent improvement over the standard quantum limit in the few-photon regime or a few dB improvement in the high power regime. However, what if phase estimation for a class of experiments is suboptimal? Depending on the measurement apparatus, phase estimation may have different fundamental limits than frequency estimation. Here we demonstrate that by using an ultra-steep, frequency-dependent gain measurement rather than performing phase estimation in a passive gyroscope, we can achieve orders of magnitude improvement below the phase-estimation standard quantum limit of a single-loop Sagnac interferometer of the same size. Further, we provide important insights into a long-debated question about the role of Doppler shifts in the Sagnac effect.

Gyroscopes are powerful tools in tests of fundamental physics, guidance systems, inertial navigation, accelerometry, geodesy, seismology and geophysics to name a few. Significant advances in micromechanical, atomic, chip-based systems and ring laser gyros have been achieved. It may come as a surprise, then, that there are still open questions about the fundamental underpinnings of gyroscopes. For the sake of clarity, we consider an optical gyroscope to be a system in which a light source and a detector, in the same reference frame, rotating at a constant angular speed, can measure the rotation rate of the system. However, instead of measuring differential phase shifts, as is typically done, we measure differential frequency shifts.

The estimation of the rotation speed is closely related to a long-debated question of the role of Doppler shifts in the Sagnac effect. In a standard Sagnac interferometer, the light is split using a beamsplitter into two counter-propagating beams that return to the same beamsplitter. Special relativity predicts an in-plane, closed-path relative phase acquired by the two beams in an optical Sagnac, given by

$$\Delta\phi = \frac{8\pi\Omega A}{\lambda c}$$

where Ω is the angular frequency, A is the gyroscope area, λ is the wavelength of light and c is the speed of light. Hence, once the phase is known, the angular rotation frequency can be determined. The shot noise limited rotation sensitivity can then be found by substituting the standard quantum limit for phase, namely

$$\Delta\phi = \frac{1}{2\sqrt{N}}$$

Where N is the number of photons.

An alternative theory is that the Doppler effect is the fundamental mechanism of the Sagnac effect. However, Malykin elucidates two reasons against the use of the Doppler effect. First, in a closed-loop system, the beamsplitter plays both the role of the emitter and the detector. He states, "...the radiation source and detector must be in motion relative to each other if the Doppler effect is to be manifest". The implies that the net Doppler shift outside the closed interferometer is zero. However, we feel this is not a good argument against a Doppler shift model, since proponents argue that it is the Doppler shifts between the source and the emitter (leading to a differential phase) that matter and not what happens external to the interferometer. We go beyond this assertion by exploring symmetry-breaking designs where the detector is not the same element as the emitter allowing us to measure differential frequency shifts even at the detector.

Malykin's second argument is that if there is a material medium, a Doppler-shift theory differs from the standard prediction by a factor of $2n^2$ where n is the index of refraction of the material. Even in vacuum, the result still differs by a factor of 2. The vacuum result is rectified by proponents of the Doppler effect by using the length of the interferometer in the interferometer's frame. However, Malykin points out that it is inconsistent to assume a Doppler shift in the lab frame and the loop length in the rotating frame.

Instead of resolving the theoretical inconsistencies, we endeavor to show that Doppler shifts do exist within the system. It is our opinion that measuring the phase alone leads to ambiguous interpretations. To parse out the role of the Doppler effect, we need a system that measures only differential frequency shifts, but *cannot* measure differential phase.

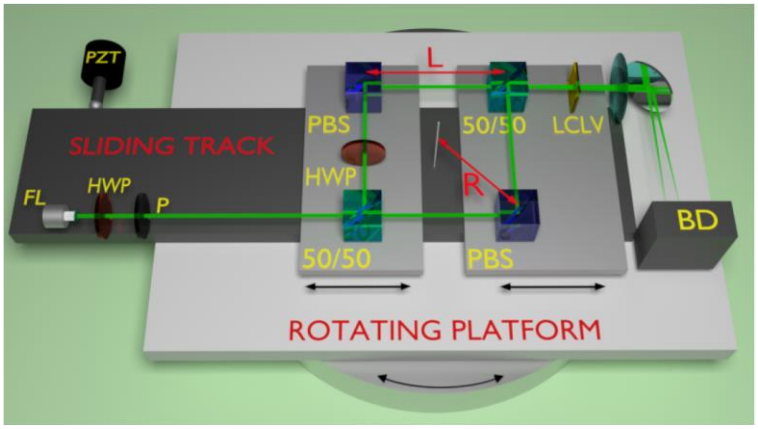

Figure 10: Experimental setup. A laser beam is coupled into a square Mach-Zehnder interferometer on top of a rotating platform. The size and distance of the interferometer relative to the axis of rotation can be controlled by moving small tables with the beamsplitters. A liquid crystal light valve acts as the relativistic "detector" by providing spectrally-dependent gain, which is then measured by balanced detectors. All elements are on the rotating platform.

For our spectral estimation technique, we incorporate an ultra-sensitive, wave-mixing spectrometer based on an extremely steep frequency-dependent gain to measure frequency offsets. We use a liquid crystal light valve (LCLV), to measure the relative Doppler shift of two counter-propagating paths, but not the relative phase. Two-beam interference in the crystal creates a self-induced index grating from which the beams scatter. The various scattering orders from the two beam-interference inside an LCLV can lead to phase-insensitive steep spectral gain dependence or extremely slow or fast group velocities. It was shown that the shot noise limited spectral sensitivity is given by

$$\Delta f = \frac{1}{|\chi|\sqrt{N}}$$

where |χ| is the slope of the spectral gain and N is the number of measured photons. Because the slope of the gain curve can be large, we can achieve very high spectral resolution. This is the type of "slow light" advantage that was sought for almost two decades.

Now, we consider the Doppler shift from each reflecting surface of a rotating interferometer, like the one shown in Figure 10. We recently showed that the Ashworth-Davies non-relativistic Doppler shift Δfm of a laser of wavelength λ from a mirror moving with angular velocity Ω and radius R is given by

$$\Delta f_m = -\frac{2\Omega R}{\lambda}\cos(\phi)\cos(\alpha)$$

where, with respect to the mirror's surface normal, α is the direction of propagation of the mirror and φ is the angle of incidence.
Consider a simple Doppler model in which the axis of rotation is at the center of a square Mach-Zehnder interferometer like the one shown in Figure 10. The distance from the axis of rotation to each reflective element is then $R = \frac{L}{\sqrt{2}}$, where L is the length of a side of the square. In this scenario the relative Doppler shifts between the two paths is given by:

$$\Delta f \simeq \frac{L\Omega\epsilon}{2\lambda}$$

The final beamsplitter, with its small relative angle, breaks the symmetry in the system. It should also be noted that the frequency differential is zero when the angle between the output beams ϵ = 0 as observed for closed systems. This model predicts, using parameters from our system, an estimated shot noise limited rotation sensitivity down to Ω ≈ 100 pRad/s/Hz−1/2 (approximately 5 orders of magnitude below the SQL for phase estimation of an interferometer of the same size and same number of measured photons).

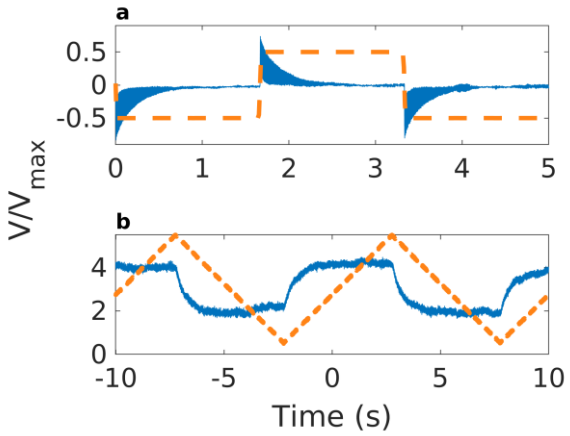

Figure 11: LCLV response vs input signals. In a, an experiment was performed similar to the one in which the laser and detector are in the laboratory frame and a mirror undergoes linear translations according to a piezo electric input signal. However, the LCLV response always reequilibrates to zero meaning the LCLV, after relaxing, has no response to constant phase. The experimental setup b utilizes the turntable shown in Figure 10 unlike a. A triangle wave is applied to the piezo-actuator which rotates the turntable yielding the expected square wave signal.

For our experiment, light from a 532 nm fiber-coupled laser was launched on a rotation mount. A half-wave plate (HWP) and polarizer (P) were used to adjust the beam intensity and make the light vertically polarized (necessary for the LCLV). The 50/50 beam splitter and a polarizing beamsplitter (PBS) were placed on a small movable platform on top of a track. The other 50/50 beamsplitter and the other polarizing beamsplitter (PBS) were placed on another movable platform on the same track. The two independently movable platforms allowed us to measure the sensitivity of the system versus the position of the axis of rotation and the interferometer's size. The two polarizing beamsplitters were used in place of mirrors allowing for amplitude control of the two paths. The beams were then directed from the polarizing beamsplitters and the final 50/50 beamsplitter such that they overlapped on the LCLV, but had a relative angle of approximately 10 mRad. The beam waists at the crystal were approximately 2.5 mm with combined intensity of between 1.5 mW and 2.5 mW impinging on the crystal. The beams then pass through a lens and are sent to a balanced detector (BD) in the focal plane of the lens where the beams have separated. The half wave plate (HWP) inside the Mach-Zehnder was adjusted until the beams were intensity-balanced in the detector. The differential balanced detector signal was passed through a low-noise preamp. From the fiber launch to the photodetectors, all equipment is on a single rotating platform atop a turntable

driven by a piezoactuator (PZT). We note that we observe the effect with the laser also in the rotating platform frame.
To test the properties of this system, we used a linear piezo-electric actuator to exert a transverse force on the sliding track that also acts as a lever arm. The horizontal distance from the PZT to the axis of rotation was 28 cm. The actuator has a linear response of approximately 60 nm/V. We used a range of amplitudes and frequencies for driving sinusoidal, triangular and square wave oscillations. To demonstrate that we are measuring a frequency offset and not a phase offset, we show that constant phase offsets (not phase gradients) do not contribute to the LCLV response. It is important to note that for demonstrating that the system is not sensitive to a constant phase offset we are not using a setup in Figure 10. Rather, the experimental setup for this experiment is based on in which a mirror is linearly translated with respect to the lab frame in which the detector and laser are stationary. Figure 11a shows the response of the LCLV to sudden changes in phase (square wave driven piezo). The Square wave peak-to-peak oscillation corresponds approximately to 17 degrees of phase shift. It can be seen that after an initial sudden change in phase (Doppler shift) the system relaxes once again to the equilibrium position (zero) even though the phase offset remains constant until the next fluctuation. This shows that the LCLV does not respond to constant phase offsets as would be the case in standard Sagnac interferometers undergoing uniform rotation. Hence, the signal must be from frequency shifts and not from phase.
We now turn to the results for the rotating platform shown in Figure 10 undergoing small oscillatory motions. As can be seen in Figure 11b, a 100 mHz triangle wave with peak-to-peak angular displacement of approximately 1 µRad is applied to the piezo actuator. At the turning points, there is a sudden acceleration at which there is a rapid change in response. After a finite crystal relaxation time, the system settles to the new equilibrium. For a system of constant rotational speed, the system approaches a constant voltage offset proportional to the speed as expected.

Figure 12 shows the driving signal and the system response of a 0.003 m^2 interferometer, from a 200 mHz sine wave (a 20 second interval is shown in the inset). The driving signal resulted in a 1.3 µRad/s amplitude for the angular velocity. The length of the total measurement was 1000 seconds. The associated amplitude spectral density of the signal is shown. It can be seen that over a large range of the spectrum, the noise floor is more than 2 orders of magnitude below the shot noise limited (the standard quantum limit) response of a standard passive gyroscope of the same area and approaches 3 orders of magnitude close to 1 Hz. Figure 13 shows the Allan deviation. The bias drift of the system is calculated to be approximately 17 nRad/s. For emphasis, we note that we are still several orders of magnitude above the shot noise limit of the frequency differential measurement of the LCLV implying that many orders of magnitude improvement are still possible.

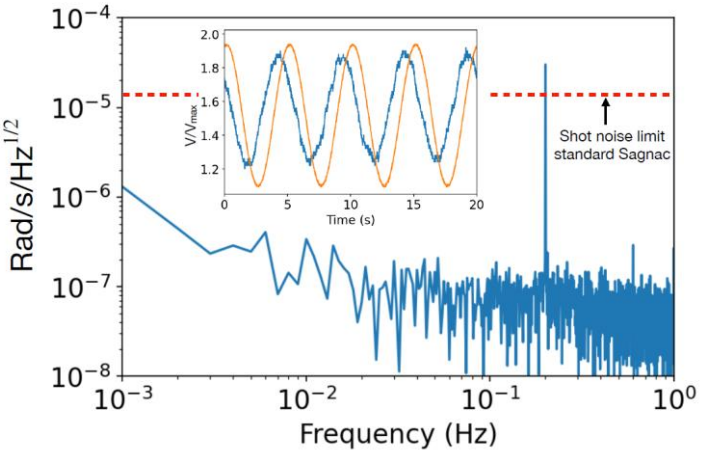

Figure 12: Amplitude spectral density of the signal response (shown in blue in the inset) of a 0.003 m^2 interferometer undergoing 200 mHz sinusoidal oscillations from the driven piezoelectric.

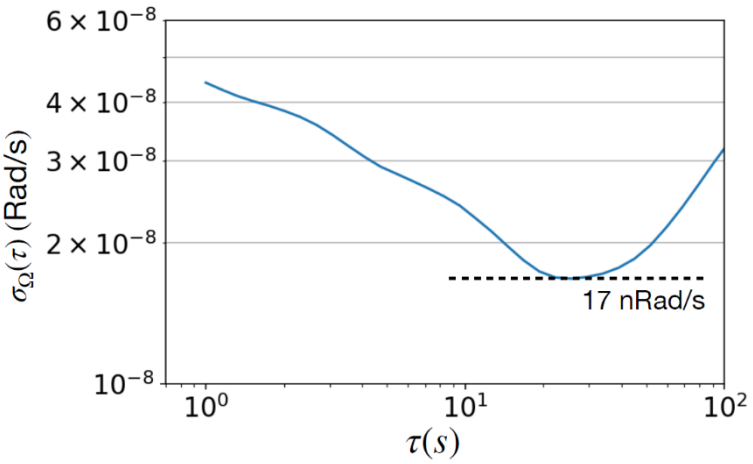

Figure 13: Allan deviation for 0.003 m^2 interferometer. The bias drift is observed to be approximately 17 nRad/s.

We tested the dependence of the system on several parameters: the position of the axis of rotation, the size of the interferometer, and the amplitude and frequency of the piezo actuated movement. For the experiments shown in Figure 14, triangle waves of various amplitudes and frequencies were used. In Figure 14a, the two movable platforms were translated together, while preserving the interferometer area, by a distance ΔL to find the system sensitivity to position of the interferometer relative to the axis of rotation. It can seen that there is a linear dependence on distance from the axis of rotation, thus differing from other passive optical gyroscopes. Figure 14b shows the dependence of the interferometer's sensitivity on the size of the interferometer. We kept one platform fixed and moved the other platform a linear distance ΔL. We plot two theoretical behavior lines to show the system sensitivity is linear in the length and not the area, which also differs from other passive optical gyroscopes. Figure 14c and d show that the response of the system is linearly dependent in the amplitude and frequency of the driving oscillation, as expected. It can be seen in Figure 14c that if the amplitude is too large, when the crystal gain curve is nonlinear, the linear behavior stops. Nonlinear behavior also occurred for oscillation frequencies above 1 Hz (not shown), which is approximately the bandwidth of the gain curve.

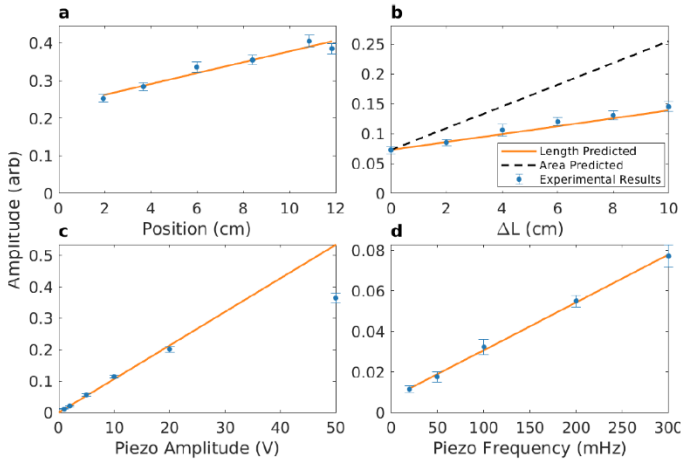

Figure 14: (a) Shows the system response as a function of a 0.003 m^2 interferometer being moved relative to the axis of rotation. b) demonstrates the dependence of the interferometer sensitivity vs a linear change in length. It can be seen that the behavior shows that the system sensitivity is a function of the length and not the area of the interferometer. c) and d) show that the system is linear in the piezo driving amplitude and frequency, respectively.

A brief discussion of some practical aspects is in order. First, the LCLV, in its current form, is very sensitive to vibrations. Second, the sensitivity and bias of the LCLV is a strong nonlinear function of the laser power. However, with intensities of even just a few 10s of mW/cm2, the transparent electrodes on the LCLV can overheat causing a liquid phase transition. This is a technical not a fundamental limitation, which can be improved. Third, air current fluctuations create temporal phase fluctuations, which appear as frequency shifts in the system. Fourth, it is likely that bias drift can be greatly improved. We believe the primary forms of bias drift were from intensity fluctuations and crystal temperature variations, both of which can be actively stabilized. Fifth, we expect the sensitivity of our device can be greatly improved if it is used in a high finesse resonator or loop design. Sixth, there are passive fiber optic gyros with similar sensitivities to ours, but with enclosed areas 10's to 100's of thousands of times larger.
The last and perhaps most important item is that we have not yet measured any signal related to the Earth's rotation. This should be manifest by a large frequency offset bias (expected to be several hundred thousand Hertz assuming a linear increase in sensitivity with distance) and a sensitivity to interferometer tilt, neither of which we have observed. We are puzzled by this and are looking for answers to large distance rotations. We note that such a large bias would be so far outside the spectral gain window that the system could not work. This dilemma could point to: 1) a flaw in the theory 2) new physics or 3) the system behaving like translational rather than rotational motion in the large distance limit. We hope this spurs additional theoretical activity in the community.

We believe we have provided compelling evidence of the possibility for enhancing sensitivity relative to some phase estimation problems by considering frequency estimation instead. We have also provided strong evidence of the role of Doppler shifts as being fundamental within the Sagnac effect. An obvious question is in what other systems such techniques could be applied. For example, it may be possible that ring laser gyros could be improved if the differential spectral estimation of the LCLV can be shown to be better than the typical heterodyne beatnote analysis.

5 References

[1] M. J. Jaroszewicz, M. Novakovic, and L. Frydman, J. Chem. Phys. **156**, 054201 (2022).